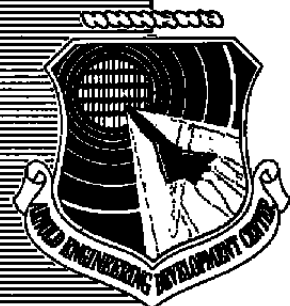# Boundary-Layer Transition on Large-Scale CMT Graphite Nosetips at Reentry Conditions

R. M. Raper
ARO, Inc.

January 1981

Final Report for Period January 26, 1978 — August 10, 1978

ARNOLD ENGINEERING DEVELOPMENT CENTER
ARNOLD AIR FORCE STATION, TENNESSEE
AIR FORCE SYSTEMS COMMAND
UNITED STATES AIR FORCE

This report has been reviewed by the Office of Public Affairs (PA) and is releasable to the National Technical Information Service (NTIS). At NTIS, it will be available to the general public, including foreign nations.

APPROVAL STATEMENT

This report has been reviewed and approved.

JOSEPH F. PAWLICK, JR., Lt Colonel, USAF
Test Director, VKF Division
Directorate of Test Operations

Approved for publication:

FOR THE COMMANDER

JOHN M. RAMPY
Technical Director
Deputy for Operations

REPORT DOCUMENTATION PAGE		READ INSTRUCTIONS BEFORE COMPLETING FORM
1 REPORT NUMBER AEDC-TR-79-45	2 GOVT ACCESSION NO.	3 RECIPIENT'S CATALOG NUMBER
4 TITLE (and Subtitle) BOUNDARY-LAYER TRANSITION ON LARGE-SCALE CMT GRAPHITE NOSETIPS AT REENTRY CONDITIONS		5 TYPE OF REPORT & PERIOD COVERED Final Report – January 26 – August 10, 1978
		6 PERFORMING ORG. REPORT NUMBER
7 AUTHOR(s) R. M. Raper, ARO, Inc., a Sverdrup Corporation Company		8. CONTRACT OR GRANT NUMBER(s) •
9 PERFORMING ORGANIZATION NAME AND ADDRESS Arnold Engineering Development Center/DOOV Air Force Systems Command Arnold Air Force Station, Tennessee 37389		10 PROGRAM ELEMENT, PROJECT, TASK AREA & WORK UNIT NUMBERS Program Element 921B03
11. CONTROLLING OFFICE NAME AND ADDRESS Naval Surface Weapons Center /WOL Naval Ordnance Laboratory Silver Spring, Maryland 20910		12 REPORT DATE January 1981
		13 NUMBER OF PAGES 42
14 MONITORING AGENCY NAME & ADDRESS(if different from Controlling Office)		15 SECURITY CLASS (of this report) UNCLASSIFIED
		15a DECLASSIFICATION DOWNGRADING SCHEDULE ·N/A

16 DISTRIBUTION STATEMENT (of this Report)

Approved for public release; distribution unlimited.

17 DISTRIBUTION STATEMENT (of the abstract entered in Block 20, if different from Report)

18 SUPPLEMENTARY NOTES

Available in Defense Technical Information Center (DTIC)

19 KEY WORDS (Continue on reverse side if necessary and identify by block number)

boundary layer transition	nosetips
laminar flow	graphite
turbulent flow	free stream
hypervelocity	radiation pyrometers
tracks	stagnation point

20 ABSTRACT (Continue on reverse side if necessary and identify by block number)

A series of tests designed to investigate the boundary-layer transition characteristics of preablated CMT graphite nosetips was conducted in a hypervelocity track facility. The location of the zone at which transition from laminar to turbulent flow occurred was measured on a number of nosetips having radii of 0.40, 0.80, and 1.125 in. The nosetips were tested at nominally 16 kfps over a free-stream pressure range of 0.13 to 0.40 atm. Transition front

DD FORM 1473 EDITION OF 1 NOV 65 IS OBSOLETE

20. ABSTRACT (Continued)

locations were inferred from nosetip surface temperature distributions obtained using a photographic pyrometry technique, and fronts were observed to range from the proximity of the stagnation point to the sonic point. It was observed that the mean transition location moved forward on the nosetip as test pressure increased. The circumferential variation about the mean transition location over a given nosetip decreased as the mean location moved nearer to the stagnation point.

AFSC
Arnold AFS Tenn

PREFACE

The work reported herein was conducted by the Arnold Engineering Development Center (AEDC), Air Force Systems Command (AFSC) at the request of the Naval Surface Weapons Center (NSWC/WOL). The NSWC project manager was Dr. Daniel C. Reda. The results of the test were obtained by ARO, Inc., AEDC Group (a Sverdrup Corporation Company), operating contractor for AEDC, AFSC, Arnold Air Force Station, Tennessee, under ARO Project Number V41G-61. The data analysis was completed on October 16, 1978, and the manuscript was submitted for publication on May 7, 1979.

CONTENTS

ILLUSTRATIONS

TABLES

1.0 INTRODUCTION

The impetus for studying nosetip boundary-layer transition is provided by ablation rates and shape change histories for currently employed reentry vehicle (RV) nosetip materials (e.g., graphite and other carbonaceous materials) dependent primarily on a complex interaction between intrinsic surface roughness and the boundary-layer flow. At high altitudes the boundary layer over the full-scale nosetip is laminar, and ablation acts to increase bluntness. Also, preferential ablation of binder elements in the surface material causes the surface to develop microroughness related to the grain size or, in the case of carbon/carbon type materials, the preform geometry. It is this microroughness that eventually causes boundary-layer transition to occur and at a higher altitude than at which it would have occurred for a very smooth surface. Boundary-layer transition results in much more severe heat-transfer rates over the region between the stagnation point and the sonic point than occur for laminar flow. The increased sidewall heat flux in the regions behind the stagnation point results in the formation of the concave nosetip shape associated with transitional and/or turbulent flows. At still lower altitudes the concave shape gives way to a sharp biconic as transition moves toward the stagnation point. Since the nosetip changes shape as the transition point moves forward, any circumferential variation in transition location can result in the formation of an asymmetrical geometry and trajectory dispersion may occur.

Experimental information required for the correct modeling of such complex phenomena is often generated in wind tunnel or arc jet environments that are incapable of achieving complete simultaneous simulation of reentry conditions in terms of Mach number, stagnation pressure, and total enthalpy. Semiempirical correlations based on such data must therefore be verified through actual flight tests. Because of the cost of full-scale testing, the inherent lack of control over the experiment, and the difficulties involved in data acquisition and evaluation, techniques that meet the verification criteria for doing subscale testing in the ballistics range have been developed. The advantage of the ballistics range in this regard is that it has the capability to duplicate actual reentry conditions in terms of simultaneous duplication of Mach number, pressure, and enthalpy for any point on a reentry trajectory. The major potential disadvantages presented by the ballistics range are limited test time and limited model scale for tests of the type described in this report.

Nosetip boundary-layer transition tests in the free-flight Range G began in 1972 in a program involving AXF-5Q graphite; a companion program for ATJ-S graphite was conducted in 1973 (Ref. 1). These tests were handicapped by shock cap radiation that obscured the low temperature laminar region, and means were subsequently devised to provide a short length of helium environment along the range centerline in which more

meaningful measurements could be obtained. Extensive tests of CMT graphite using this technique were conducted with both smooth and preablated nosetips. The preablated specimens were produced by exposing the test articles in the AEDC 5-MW Arc Jet for several seconds to establish a characteristic surface roughness before launching the test articles in the range. The very different results (not available in the open literature) that were obtained for the two types of nosetips indicated that, at least for CMT graphite, apparently very different results were usually produced for nonpreablated surfaces. The initially smooth-surface response was generally characterized by hot spots and a transition front that was grossly irregular and did not necessarily extend completely around the nosetip. The preablated nosetips produced the more symmetrical patterns one would expect.

The objective of the present test program was to obtain more and higher-quality transition data for CMT nosetips with radii approaching those of full-scale RV's. Because of the previous results for this material, only preablated test specimens were tested. In addition, the recent availability of track guidance for test models has relieved the aerodynamic stability constraint on model design and permits much larger nosetips to be tested. Other advantages offered by model guidance are that (1) the test specimens may be recovered for posttest evaluation of surface roughness and (2) the elimination of trajectory dispersion makes it possible to obtain higher resolution photographic pyrometry data. These advances in test technique have greatly enhanced the capabilities of the range in nosetip transition testing.

It is the purpose of this report to present new and improved-quality transition data that have been obtained for near full-scale CMT graphite nosetips as described above. These results are interpreted in terms of mean transition location. The asymmetric nature of the transition process is described statistically.

2.0 APPARATUS

2.1 TEST UNIT

The present test program was conducted in the AEDC Hypervelocity Range/Track (G) facility. This test unit is basically the free-flight Range G (Ref. 2) that has been equipped with a removable track model guidance and recovery system (see Fig. 1). Hence, the facility can be operated in either a free-flight mode or track mode. The primary components of the facility in the track mode are (1) a model launcher that consists of a 2.5-in.-caliber, two-stage light-gas (H_2) gun approximately 150 ft long, (2) a model guidance system that consists of ninety-one 10-ft-long track sections, (3) a model recovery device that is a 500-ft-long tube in which the model is aerodynamically decelerated, (4) the 1,000-ft range tank that encloses

the track and provides the desired test environment, and (5) an instrumentation system capable of in-flight data acquisition. Bulkheads are located in the range tank at 85 and 390 ft from the uprange end; openings in the bulkheads through which the track passes are equipped with quick-opening valves. These allow staged test pressures along the flight path if desired. Other quick-opening valves are installed along the the recovery tube to maintain its helium and nitrogen gases at the required pressure before model arrival. A more complete description of the track system and its operation is given in Ref. 3.

2.2 INSTRUMENTATION

2.2.1 Photographic Pyrometry

In-flight nosetip surface temperature measurements, the primary data in this test program, were obtained by means of photographic pyrometry. This temperature measurement technique involves basically the following sequence: (1) a high-speed, image-converter camera system is used to obtain a stop-motion, self-luminosity photograph of the test model in flight, (2) calibration data from a carbon arc (or tungsten) reference source are recorded on identical film and are processed simultaneously with the model photograph, and (3) densities on the film image of the model surface are measured and converted to temperatures using the calibration data.

Temperatures measured by this method are brightness temperatures if the radiation observed is strictly incandescent radiation. In general, true surface temperatures may be calculated if the emissivity of the test material is known. In most instances, test materials of current interest are carbon and graphite compounds with emissivities very near unity. In these cases, temperatures measured are surface temperatures accurate to within the measurement uncertainty of the systems.

The manner in which photographic pyrometry systems are employed in the track mode of testing for in-flight model surface temperature measurements is shown schematically in Fig. 2. The near head-on view angle is highly advantageous for transition testing because it offers the best possible coverage of the subsonic portion of the flow field. Two types of proximity-focused image-converter cameras are used. One employs fiber-optic coupling from phosphor anode to the recording film (Generation I, or Gen-I, image intensifiers), and the other type features a microchannel plate amplifier between photocathode and phosphor anode (Generation II, or Gen-II, image intensifiers). Both types of intensifiers have S-20R spectral response: They respond to visible and near-infrared radiation to a wavelength of approximately 0.93 μm. In terms of applications, the most important difference between the two types of intensifiers is that the Gen-II type is more sensitive than the Gen-I type (see

Table 1). For instance, for an exposure duration of 1,000 nsec, the Gen-II system threshold is 1,250°K, whereas for the Gen-I system it is 1,600°K. However, the dynamic range of the Gen-I is smaller than that of the Gen-II. For the present test program, the wide range of nosetip sizes and test conditions that were used resulted in a wide range of temperature levels at a given station location. For this reason, the five range locations available for pyrometry instrumentation (Stations 4, 11, 20, 29, and 41, which are 100, 238, 398, 596, and 836 ft from range entrance, respectively) were equipped with different systems consistent with the expected nosetip temperature range. However, for shots utilizing the largest nosetips, the temperature levels generally did not reach the threshold of even the Gen-II systems until the model had reached station 20. Consequently, for most of those shots, only three Gen-II systems could be operated.

For almost all shots in the present test program, the brightness temperature of the air shock cap exceeded the nosetip surface temperature over the full flight distance. When this condition exists, use of the measurement technique herein described requires elimination of shock cap radiation. This problem was solved in previous free-flight tests by providing a small chamber filled with helium at each measurement station. Each chamber was opened immediately preceding model arrival so that measurements could be obtained in the helium environment. The advantage of a helium environment is that its radiation intensity is much lower than that for air for the velocity and pressure conditions desired for the present test. The shock cap quench technique developed for track testing uses a plenum that is suspended from the track tube and that vents a low-velocity column of helium vertically through the slots in the track tube. This system provides a helium environment of 95 + percent purity over a flight distance of 10 in. The model is photographed near the end of the helium-rich region. Such systems were used at stations 11 and 29 for all the present tests. For stations 4, 20, and 41, the track tube slots were lengthened so that four of the 1-ft plenums could be utilized end to end. The purpose of this was to provide greater flow-field quench distances to minimize extraneous model and wake luminosity, a condition that was required for another test program. The 1-ft-sweep distance was sufficient to quench nosetip flow fields. Evidence of this is provided by stagnation point temperatures down to the threshold of the pyrometry systems being measured at some test conditions in which the air shock cap temperature with no quench would have been much higher.

2.2.2 Laser Photography

Laser-lighted photography was used as part of the standard instrumentation to obtain high-resolution in-flight photographs of test articles. The intensity of the light source permits extremely brief exposure times (20 nsec) and effectively eliminates motion blur. For ablation and erosion tests, laser photography provides the means to obtain in-flight surface

recession data. For the present test program, the role of laser photography was to evaluate the in-flight quality of the model nose test surface.

A typical laser photographic system for track applications is shown schematically in Fig. 3. This optical arrangement provides a combination of diffuse front and back lighting through appropriate slots in the track tube. This system produces a magnification of approximately 0.7. Peak photographic resolvability has been shown to be approximately 25 μm. In contrast, the resolution of the laser photography systems configured for the free-flight mode of testing is 200 μm.

2.3 MODEL DESCRIPTION

The three model configurations shown in Fig. 4 were required to accommodate the different sizes of nosetips tested. Only one shot was made with the 0.40-in. nosetip (Fig. 4a), and most of the present shots used the model configuration shown in Fig. 4c. This configuration features a hemispherical nosetip ($r_n = 1.125$ in.) nearly as large in diameter as the launch tube, therefore representing the maximum model size. Such a model was not suitable for free-flight testing because the aerodynamic stability requirement for free-flight models could not be satisfied within the launcher-imposed weight limit.

The method of model recovery in the track guidance system imposes a model design constraint: The test article must retain sufficient structural integrity at the end of its flight to withstand deceleration loading. Initially, most of the track models used in materials testing were similar to that shown in Fig. 4a. With this model design, the test material configuration is a reverse-taper plug that is swaged in place in the model forebody. Larger nosetips, which were required for expanding the range of diameters, could not survive launch loading in a plug configuration because of the low tensile strength of graphitic materials. Thus, large nosetips ($r_n \approx 1$ in.) were constrained to follow a thin shell design. The difficulty posed by this configuration is that the only practical means by which a shell may be attached to a substrate material is a chemical bond (epoxy), which can be expected to weaken at about 200°F. This problem was addressed by parametric calculations of the back-face temperature of the shell for a range of thicknesses and exposure times. A wall thickness of 200 mils was sufficient to contain the back-face temperature below 200°F for a 60-msec test duration and a 30-msec recovery cycle duration. The thermal response of the surface for this thickness was essentially the same as that for a semi-infinite wall thickness. Small carbon-carbon pins were included in the model design to hold the cap in place after model motion had been arrested and after the back-face temperature had been driven by conduction of heat from the hot surface region to beyond the bondline limit. Another purpose of the pins was to provide hot spots at known surface locations for data reduction purposes. This is discussed further in Section 4.2.

The ballistic characteristics of the three model configurations (nose radius, r_n) utilized in this test program are summarized below:

r_n, in.	Weight, gm	C_D^*	β^*, lb/ft^2
0.40	510	0.43	76
0.80	532	0.60	57
1.125	619	0.84	48

*Includes track friction drag (C_D obtained using velocity measurements from X-ray stations)

The CMT graphite nosetip test specimens utilized in the present test series were fabricated at AEDC from billet Nos. 104C-04, 103J-15, 104K-08, and 104K-15 supplied by the Navy.

3.0 TEST PROCEDURE

3.1 TEST TECHNIQUE

The basic test technique used in the present program was to launch the model on the track at a specified range pressure and velocity and to obtain brightness photographs of the nosetip at selected locations along its flight path. As the nosetip moved down the range, its surface temperature—and brightness—increased in accordance with the distribution of heat input over its surface. The temperature distribution data were obtained directly from the brightness photographs. Transient temperature measurements plus calorimetric properties of the test material provide sufficient data for inferring the actual convective heat-flux distribution.

All the nosetips tested during this program were preablated in the 1-mw APG Vacuum Facility of the Acurex Corporation. These runs were made at a centerline enthalpy of about 43,000 btu/lb and a reservoir pressure of 0.06 atm. The exposure durations and resulting surface recession levels varied with model geometry as follows:

r_n – Initial, in.	r_n – After Arc Run, in.	Exposure Time, sec	Stagnation Point Recession, in.
0.40	0.43	20	0.035
0.80	0.90	61	0.063
1.125	1.25	72	0.062

Considerable care was taken to preserve the surface roughness features developed in the arc jet. To assure that each nosetip surface was undamaged, each was inspected and photographed before being loaded in the launcher. The nosetips that were recovered intact were photographed and then shipped to the NSWC as directed.

3.2 DATA REDUCTION

A self-luminosity photograph was obtained for each model as it passed through the field-of-view of each image-converter camera. This photographic negative and a calibration negative—produced by photographing with the same camera using either a carbon-arc light source or a tungsten source, depending on the desired calibration range—were simultaneously developed. These negative pairs were then processed on a high-speed, digital-scanning microdensitometer that stored on magnetic tape the film density distribution for the nosetip image and the density-versus-temperature data from the calibration images. These data were then computer processed to produce a thermal contour map of the nosetip. Next, a computer drawing of the nosetip shape as it would be viewed by an image-intensifier camera was superimposed on the contour map so that the hot spots caused by the marker pins coincided with their known locations. Aligning these known surface points established the geometric center of the nosetip. The contour map representation is in film plane coordinates; however, a procedure has been recently implemented to transform the film plane data to spherical coordinates. Thus, the final temperature data consisted of a computer-generated tabulation of the temperature distribution along each of 120 rays spaced at 3-deg intervals around the nosetip for each photographic pyrometry station. A flow chart of this data reduction procedure is shown in Fig. 5.

3.3 DATA UNCERTAINTY

The uncertainty model employed to evaluate the experimental results subsequently presented consisted of two parts: bias error and precision error. Their sum defines the total measurement uncertainty. The following are estimates for measurements of free-stream pressure, temperature, and velocity:

<u>Estimated Uncertainty, 2σ</u>

Parameter	Bias, percent	Precision Error percent	Total Uncertainty, percent
Free-stream pressure, p_∞	0.7	0.3	1.0
Free-stream temperature, T_∞	0.1	0.2	0.3
Free-stream velocity, V_∞	Negligible	0.3	0.5
Stagnation enthalpy, H_o	Negligible	1.0	1.0
Stagnation pressure, p_o'	0.8	1.2	2.0

The uncertainty involved in measuring the surface temperature at a specific location on a nosetip has also been assessed. This uncertainty arises primarily from (1) relating points viewed in the film plane to actual spherical nosetip surface locations and (2) measuring the temperature at a given point in the film plane. The model image in the film plane contains four known surface locations; these are the previously described hot spots caused by marker pins. The location uncertainty occurs in aligning these marker spots with their known locations. Uncertainty in this alignment is estimated to result in a stagnation point location uncertainty of about 0.04 in. A location bias error of up to 1.7 deg in the flow direction could be incurred in transforming the film plane data to spherical coordinates. Measurements of surface temperature at a given film plane location are derived using a densitometer with a 100-μm aperture. Near the stagnation point, where the nosetip surface is most nearly parallel to the film plane, this aperture size corresponds to a streamwise angle increment of 0.4 deg; the temperature is an average value over this region. The magnitude of the resulting precision error is dependent on the temperature gradient.

The precision with which the photographic pyrometry systems can measure a given uniform temperature was determined from static measurements of a standard carbon-arc light source. The system precision error associated with temperature measurements, shown in Fig. 6, varied with temperature level. The main sources of uncertainty are gradients in gain across the face of the image intensifier and microdensitometer imprecision (± 0.01 D). As shown in Fig. 6, uncertainty increases toward the high-temperature end of each dynamic range for each photopyrometer. This is a consequence of the particular relationship of the reciprocal of temperature with film density (approximately linear). For a given uncertainty in film density, the corresponding uncertainty in temperature is considerably greater for the higher temperatures (lower densities).

A test-related source of error not previously discussed is an image-intensifier characteristic called flare. Light reflections inside the intensifier create very bright image areas that contribute noise illumination to adjacent areas of the displayed image; i.e., a bright spot will have a halo around it. Troublesome flare effects can produce significant uncertainty in surface temperature measurements. These flare problems arise from test-related sources—excessively hot surface areas on the nosetip, heat shield luminosity, and wake radiation. In flare-dominated photographs, it is not possible to extract certain low temperature data, so it is very important to minimize flare sources. Figure 6 characterizes the overall uncertainty associated with surface temperature measurements made in the absence of significant flare.

3.4 AEROTHERMAL ENVIRONMENT

The aerothermal environment for a ballistics range test article is specified by the test gas composition and its static temperature, its static pressure, and the model velocity. For all but one of the shots reported herein, the test gas was air (nominally at 76°F). That one shot was made with nitrogen as the test gas at the same nominal static temperature as the air shots. The nominal launch velocity for all shots was 16 kfps, and the actual velocity ranged from 15.8 to 16.2 kfps (expect as noted in Table 2). The corresponding nominal stagnation enthalpy was 5,100 Btu/lb, and the stagnation pressure ranged from 33·atm for $p_\infty = 100$ torr to 100 atm for $p_\infty = 300$ torr. The velocity of the test model at any flight distance may be calculated from the ballistics characteristics of the configuration and the test conditions using the following equation:

$$V_\infty = V_{\infty_i} \, e^{\left(-4.87 \times 10^{-5} \, p_\infty x / \beta \right)}$$

with p_∞ in mm-Hg, x in ft, and β in lb/ft². With this equation, the velocity decays for three test pressures for the large nosetip model were calculated and are shown in Fig. 7.

4.0 EXPERIMENTAL RESULTS

Twenty-seven shots were fired during the present test program. The test summary, shown in Table 2, indicates that 18 shots produced data of sufficiently high quality to be considered for analysis. The experimental results that are discussed in this section for these shots are in-flight laser photographs, image-intensifier camera photographs, thermal contours, and mean surface temperature distributions.

4.1 IN-FLIGHT LASER-ILLUMINATED PHOTOGRAPHS

During this test program the in-flight laser photography capability described earlier was utilized to determine whether the test specimens were damaged during launch. Because of the sensitivity of boundary-layer transition to surface imperfections, the preablated surface characteristics had to be preserved except for ablation effects. The small polyethylene particles, present in the track tube after each shot, that were swept up by the launcher muzzle blast and consequently impacted on the nosetip were the main cause of damage to the test surface. The muzzle blast preceded these models for about 30 ft following launcher exit for most test conditions; therefore, it was only over this 30-ft interval that damage occurred. Though the entire track housing was routinely cleaned before each shot, special emphasis was given to the uprange end once the cause of the damage was discovered. Examples of surface damage are shown in Fig. 8. For two of the·shots (5,014 and 5,043) the

13

damage was so extensive (Fig. 8a) that the data were judged to be useless. For several other shots (5,038, 5,044, and 5,063) the damage was minimal (Fig. 8b), and the data were judged to be acceptable although data for surface rays containing craters are questionable. Most of the shots were undamaged; their surfaces resembled the example in Fig. 8c. The small size of the damaging particles and the fact that they were generated during every launch by the destruction of the pump tube piston combined to make it impossible to establish an absolutely debris-free condition in the track tube.

4.2 IMAGE-INTENSIFIER CAMERA PHOTOGRAPHS

Some information concerning the presence and location of transition fronts for CMT graphite nosetips is apparent in the image-converter camera photographs, examples of which are shown in Fig. 9. The most significant feature of these photographs is the bright ring surrounding the darker central region of each nosetip. The relatively dark (cool) center of each image corresponds to a region of laminar flow, whereas the relatively bright (hot) region encircling it defines a zone of transitional/turbulent flow. This is in accordance with the well-known laminar/turbulent heat-transfer distribution over a hemisphere. Only when a boundary layer is entirely laminar and, hence, there is no transition zone on the nosetip, does the ring not occur. The point at which the brightness distributions change from dark to light in each of a series of photographs may be somewhat misleading. The response characteristics of the individual tubes and the modes in which they are operated give rise to some of the apparent differences. However, for a given photograph, the circumferential variation in the "brightness onset" location is significant since it occurs at approximately the same temperature around a nosetip.

For the single 0.40-in. nosetip that was tested (Shot No. 5,000), the transition zone was near the stagnation point initially, but then it gradually disappeared with time. For the other, larger nosetips, such dramatic changes in transition zone location were not observed. At a pressure level of 100 torr (Shot No. 5,021) a transition zone was only barely established near the sonic point. All other shots demonstrated a well-established transition zone at the first measurement station, and its location tended to move toward the stagnation point as the test pressure was increased.

To derive spatially resolved temperature distributions from these photographs, a provision was made for producing bright spots at known surface locations directly on each nosetip photograph. This was accomplished by having the four nosetip anchor pins—spaced 90 deg apart around the nosetip and located 60 deg off its centerline in the flow direction—protrude 0.050 in. above the surface. Extending outside the boundary-layer thickness, the pins were subjected to severe heating and were consequently much hotter than the surrounding surface. These pins were clearly visible in all the image-intensifier camera

14

photographs* and provided the reference points necessary to determine the geometric center of the nosetip image.

It is evident in some of the photographs, particularly those from Shot Nos. 5,038 and 5,044, that the transition zone was not very symmetrical relative to the stagnation point. This could possibly be a consequence of angular motion of the model. It is unfortunate that, because the model was surrounded by the track tube, the 53 orthogonal shadowgraph systems used in free-flight tests to record model motion were not usable. However, during these tests the model was photographed through the slots in the track tube at ten range locations using X-ray systems. Seven of these systems—positioned laterally—viewed the model from a horizontal direction, thus recording angles in the pitch plane. The other three—positioned superiorly—viewed the model from above, thereby observing yaw plane motion. Though orthogonal views would have been desirable, the data shown in Table 3 are sufficient to indicate that the model angle of attack was usually less than 1 deg. However, this level was exceeded at some time during every shot. The nature of this motion is presumed to be random wander of the model back and forth between the rails. The mean of all the angles measured at different locations indicates that angular displacement may have peaked somewhere near midrange.

4.3 THERMAL CONTOURS

Following application of the microdensitometer processing technique earlier described, the photographic images presented in Fig. 9 were computer-plotted as thermal contour maps. Several examples of these maps are shown in Fig. 10. Since they are drawn in film plane coordinates, they are a quantitative representation of the photographs. The contour interval is 100°K; a heavy contour line denotes 500°K intervals. One purpose of the contour maps is to so quantify the temperature gradients that were apparent in the photographs that test results can be rapidly surveyed. In addition, the approximate location of the transition front is made readily apparent by the contour line spacing; i.e., the region of the closest spacing of the contour lines corresponds to the zone over which heating rate increases from laminar to turbulent levels.

A refinement of the contour map presentation produced for each nosetip photograph was obtained by transforming the digital temperature data into spherical surface coordinates. An example of the resulting data is shown in Fig. 11 for station 20 of Shot No. 5,045. Here the circumferential location (around the nosetip) is given in the first column, and listed in the first row is the angular location in the flow direction (3 to 75 deg). The

---

*Pins were installed on the nosetip for Shot No. 5,000 because of the small size.

angular increment in either direction is 3 deg. Note that a single row of measurements defines the temperature distribution along one ray. Finally, the mean temperature values along with the standard deviation of the individual circumferential measurements (at each location in the flow direction) are tabulated in the last two lines. These data were compiled on magnetic tape in this same format and have been examined ray by ray using the interactive graphics techniques described in Ref. 4. A transition location as defined in Fig. 12 for a typical temperature distribution was tabulated for each ray of each nosetip image. The objective of this work, described by Reda and Raper in Ref. 5, was to quantify the variations in the transition front locations that are apparent from the contour maps. The data from each photograph yielded 120 transition location measurements, example plots of which are shown in Fig. 13, and from these measurements a mean transition location, $S/r_{n_{TR,mean}}$ was calculated. As shown in Fig. 14 (also Fig. 14 in Ref. 5), the mean transition location progressed toward the stagnation point as the range pressure was increased. A parameter used to further characterize the transition-front variations was the standard deviation (σ_{tr}) of the 120 circumferential measurements about the mean transition location. An asymmetric transition front location (characterized by σ_{tr}) and the associated asymmetric heating distribution can result, in flight, in a longer term, ablation-induced nosetip asymmetry with potentially serious implications for vehicle accuracy. As shown in Fig. 15 (also Fig. 15 of Ref. 5), the mean of the σ_{tr} measurements decreased as the mean transition location moved forward. The data shown in Figs. 14 and 15 were derived only from photographs for which the transition front had not yet begun to shift rearward (during a flight). Thus, more emphasis was placed on uprange data than on that obtained later in a flight.

5.0 SUMMARY OF RESULTS

A series of tests to investigate the boundary-layer transition characteristics of preablated CMT graphite nosetips was conducted in the AEDC Hypervelocity Range/Track (G). The nominal test velocity was 16 kfps, and free-stream pressures ranged from 0.13 to 0.40 atm. Three different sizes of nosetips were tested, r_n = 0.40, 0.80, and 1.125 in. The results indicate the following:

1. Measured transition-front locations on the hemispherical nosetips varied from the proximity of the stagnation point to the sonic point; transition moved forward on a nosetip as the test pressure was increased.

2. The magnitude of deviations in the transition-front location data—as defined by σ_{tr} measurements—decreased as transition moved forward on a nosetip.

3. Nosetips with radii approaching those of full-scale RV's can be successfully tested in the ballistics range at velocities and pressures duplicating reentry conditions, and they can be recovered intact for posttest examination.

4. Test articles can be preablated to improve the reentry simulation without significantly degrading their strength.

5. The addition of protuberances near the aft end of the test surface provided a valuable geometric reference that enhanced the data quality because the stagnation point location uncertainty was reduced.

REFERENCES

1. Miller, John T. "Nosetip Transition Measurements in a Reentry Test Environment." AEDC-TR-76-118 (ADB013270L), August 1976.

2. *Test Facilities Handbook* (Tenth Edition). "Von Kármán Gas Dynamics Facility, Vol. 3." Arnold Engineering Development Center, Arnold Air Force Station, Tennessee, July 1971.

3. Norfleet, G. D., Hendrix, R. E., and Jackson, D. "Development of a Hypervelocity Track Facility at AEDC." American Institute of Aeronautics and Astronautics, Aerospace Sciences Meeting, 15th, Los Angeles, Calif., January 1977, AIAA Paper No. 77-151.

4. Reda, Daniel C. and Brown, Hensel, S. "Analysis of Nosetip Boundary-Layer Transition Data Utilizing Interactive Graphics." *Instrumentation in the Aerospace Industry—Vol. 24/Advances in Test Measurement—Vol. 15, Part Two, Proceedings of the 24th International Instrumentation Symposium—Albuquerque, N.M.* Publications Department, Instrument Society of America, Pittsburgh, Penn., 1978, pp. 515-524.

5. Reda, Daniel C. and Raper, Richard M. "Measurements of Transition Front Asymmetries on Large-Scale, Ablating Graphite Nosetips on Hypersonic Flight." American Institute of Aeronautics and Astronautics, 17th Aerospace Sciences Meeting, New Orleans, La., January 1979, AIAA Paper No. 79-0268.
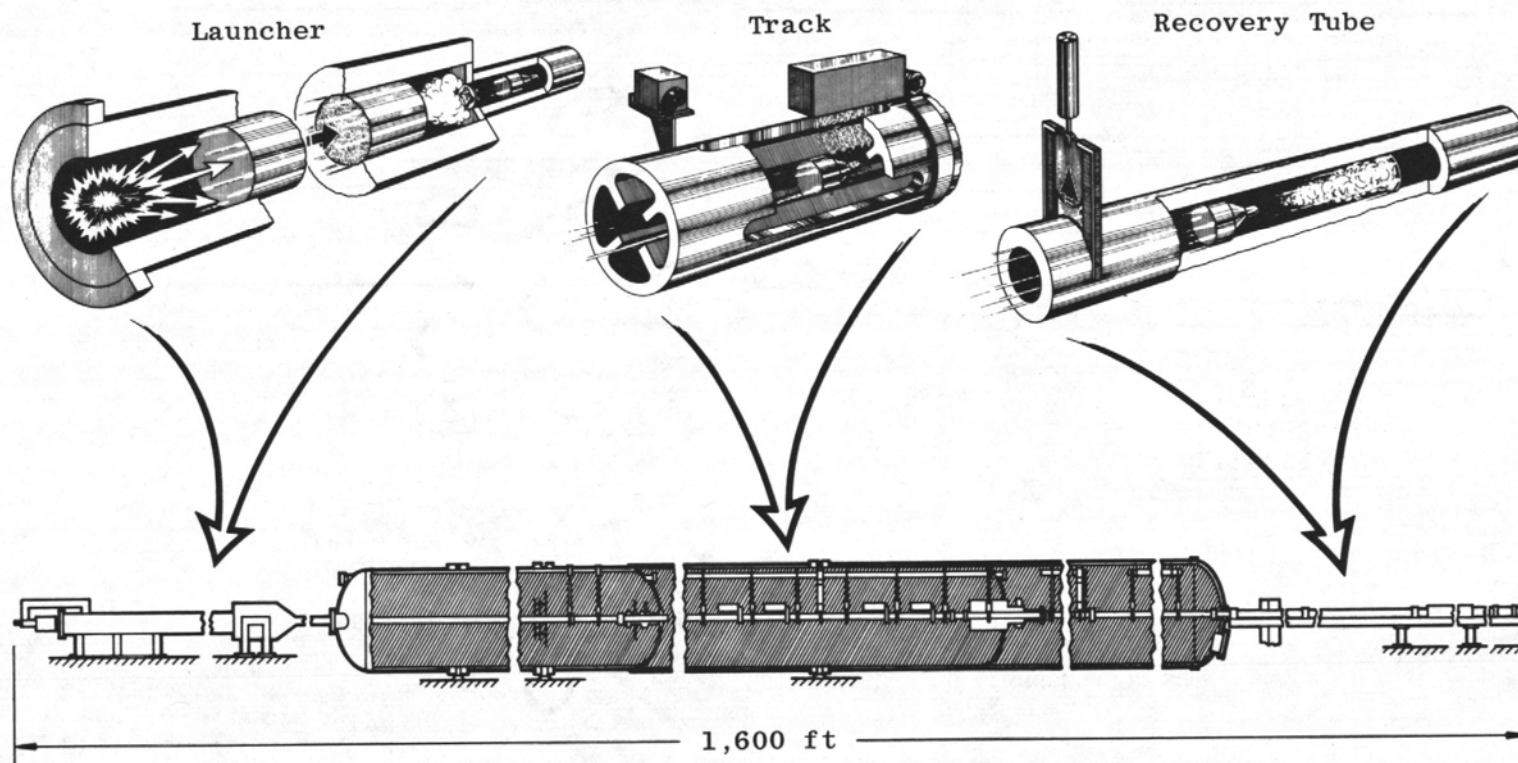
Launcher

Track

Recovery Tube

|— 1,600 ft —|

Figure 1. AEDC, 1,000-ft Hypervelocity Range/Track (G).

Notes:

1. Distance along Optical Axis from Camera Lens to Focal Plane: 34.5 in.
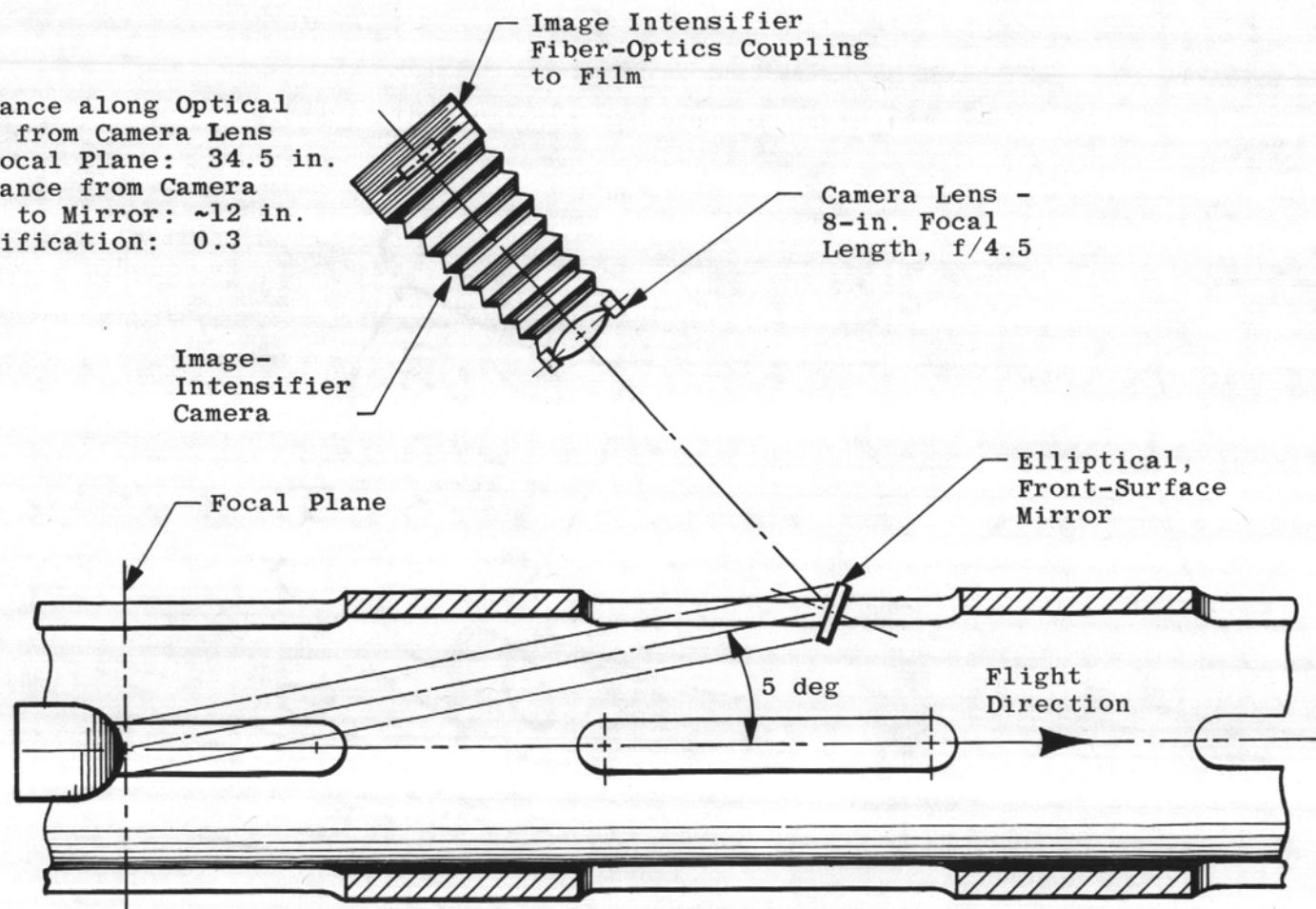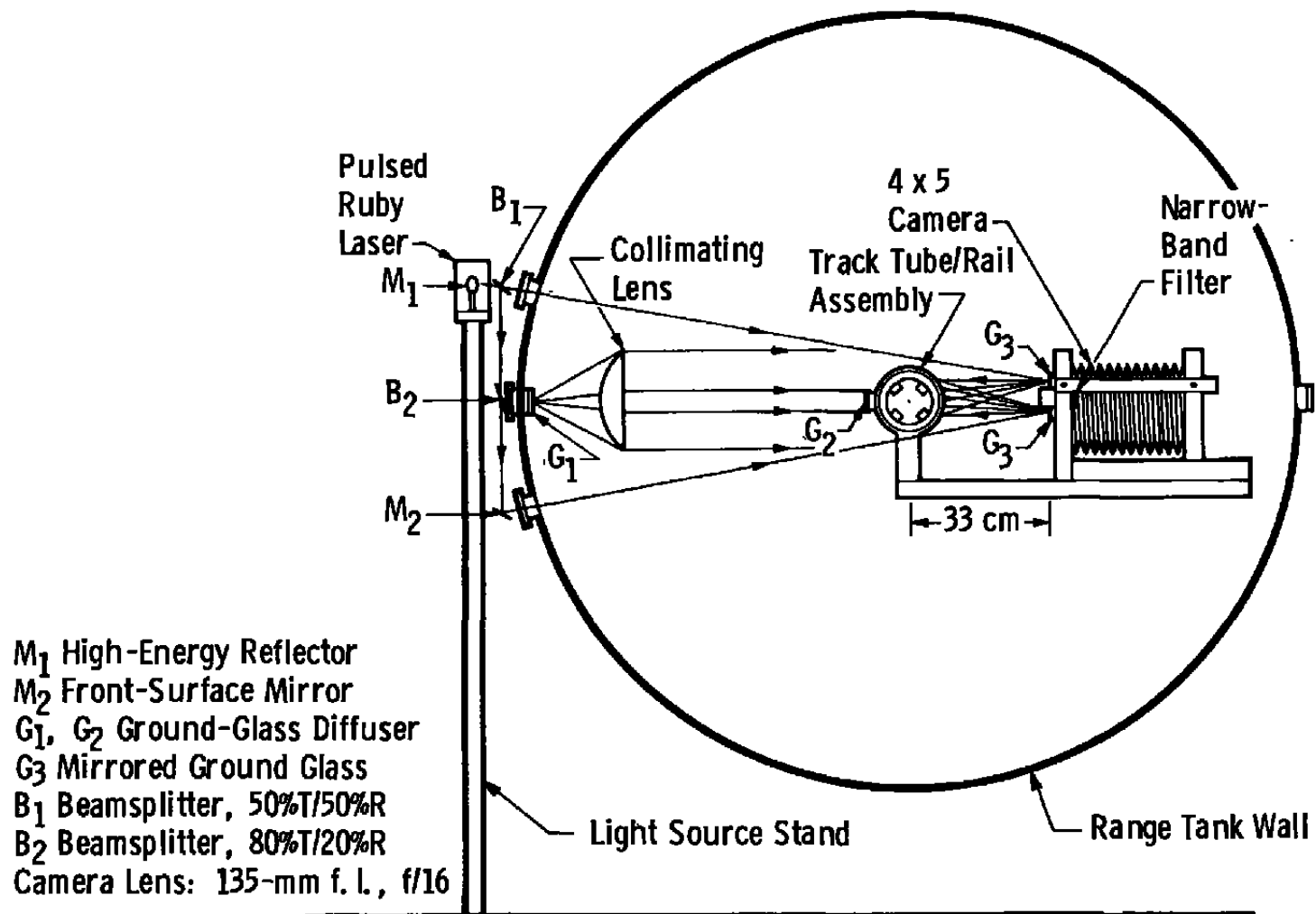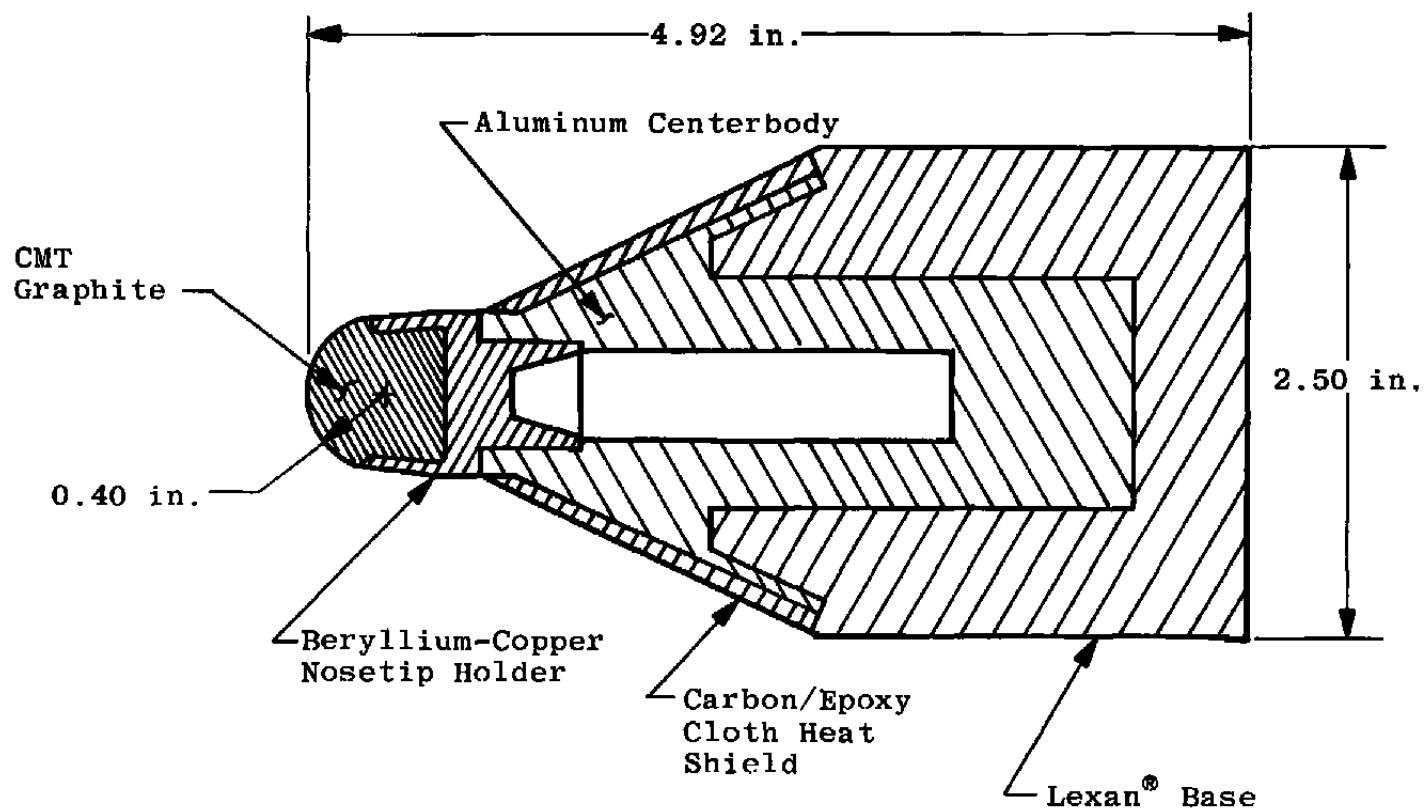2. Distance from Camera Lens to Mirror: ~12 in.
3. Magnification: 0.3

Image Intensifier Fiber-Optics Coupling to Film

Camera Lens – 8-in. Focal Length, f/4.5

Image-Intensifier Camera

Elliptical, Front-Surface Mirror

Focal Plane

5 deg

Flight Direction

Figure 2. Track G photopyrometer system.

Pulsed
Ruby
Laser

B_1

M_1

B_2

M_2

Collimating
Lens

G_1

4 x 5
Camera
Track Tube/Rail
Assembly

G_2

G_3

G_3

Narrow-
Band
Filter

←—33 cm—→

M_1 High-Energy Reflector
M_2 Front-Surface Mirror
G_1, G_2 Ground-Glass Diffuser
G_3 Mirrored Ground Glass
B_1 Beamsplitter, 50%T/50%R
B_2 Beamsplitter, 80%T/20%R
Camera Lens: 135-mm f. l., f/16

Light Source Stand

Range Tank Wall

Figure 3.   Track G front-light/back-light laser photography system.

a. $r_n = 0.40$ in.
Figure 4. Nosetip transition models.

5.15 in.

Marker/Anchor
Pins (4)

0.80 in.

CMT Graphite
~0.20 in.

Aluminum
Centerbody

2.50 in.

Heat Shield

Lexan® Base
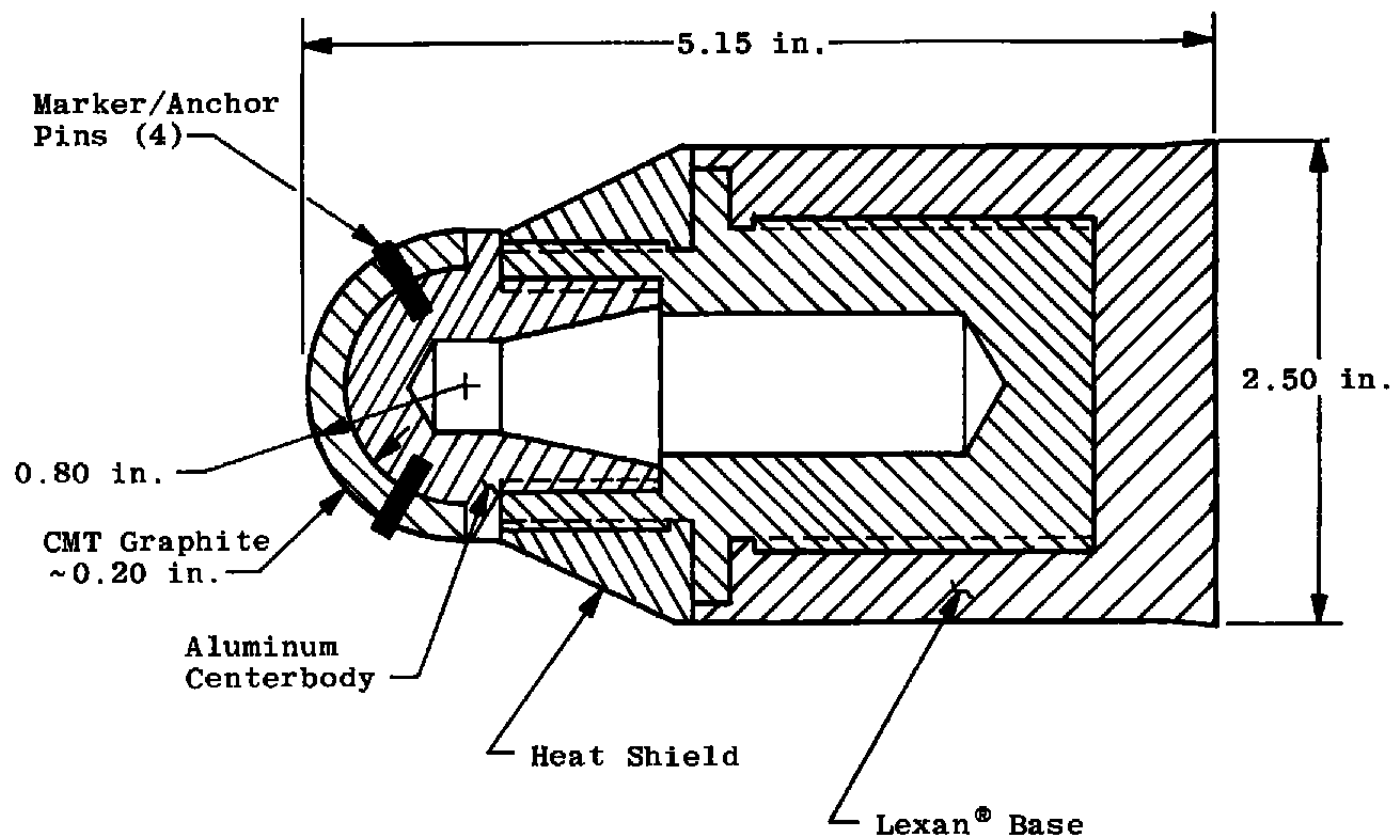
b. r_n = 0.80 in.
Figure 4.   Continued.
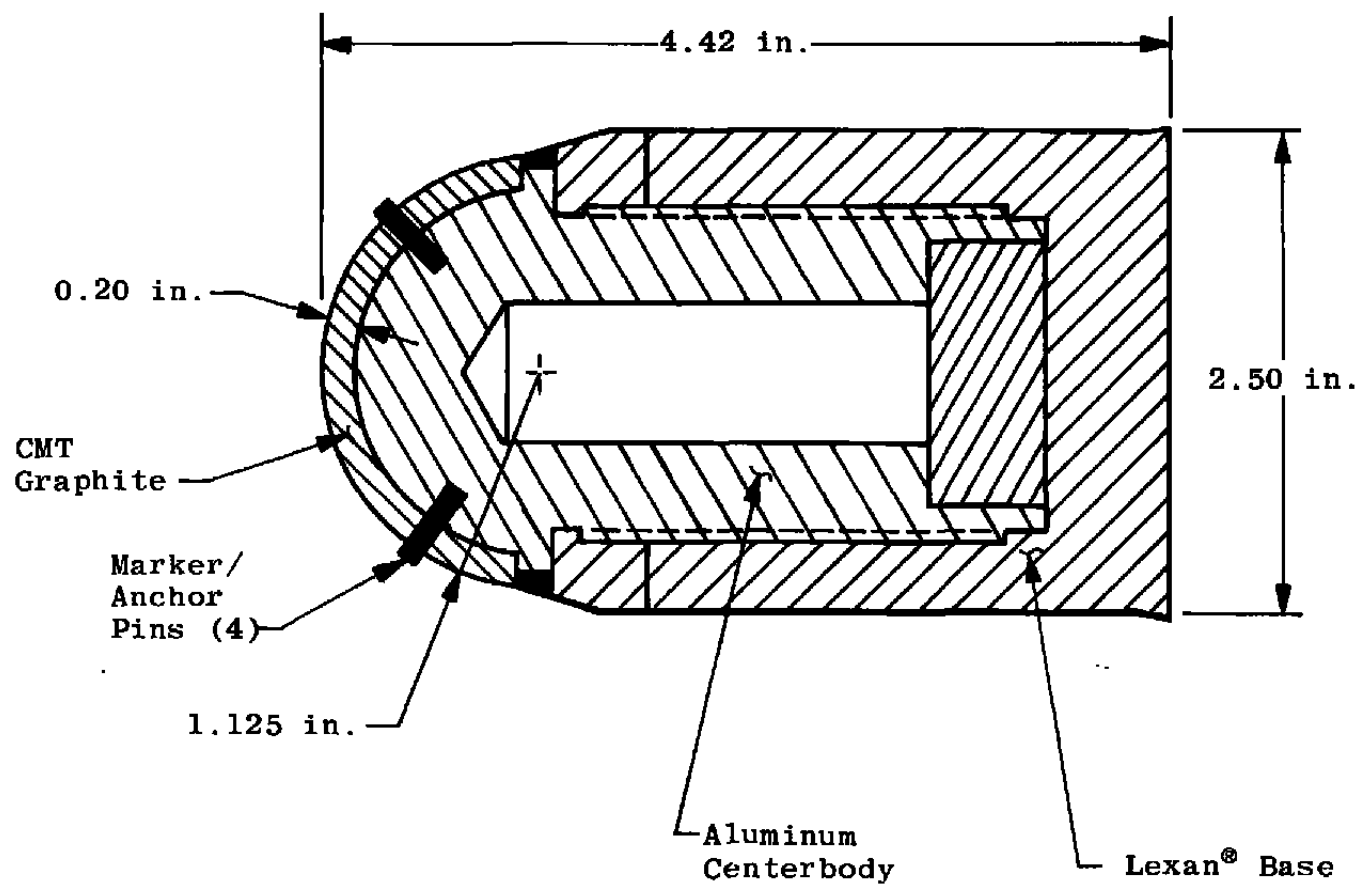
c. r_n = 1.125 in.

Figure 4. Concluded.

Developed
Negatives

| Image-Converter Camera | → Exposed Film (Data and Calibration) → | Darkroom Processing | → | Digital Scanning Microdensitometer |

Mag. Tape Unit

Computer

Density Contours

Calibration Curve

Density / Temperature

Temperature Contours

Tabulated Data
in Spherical
Coordinates
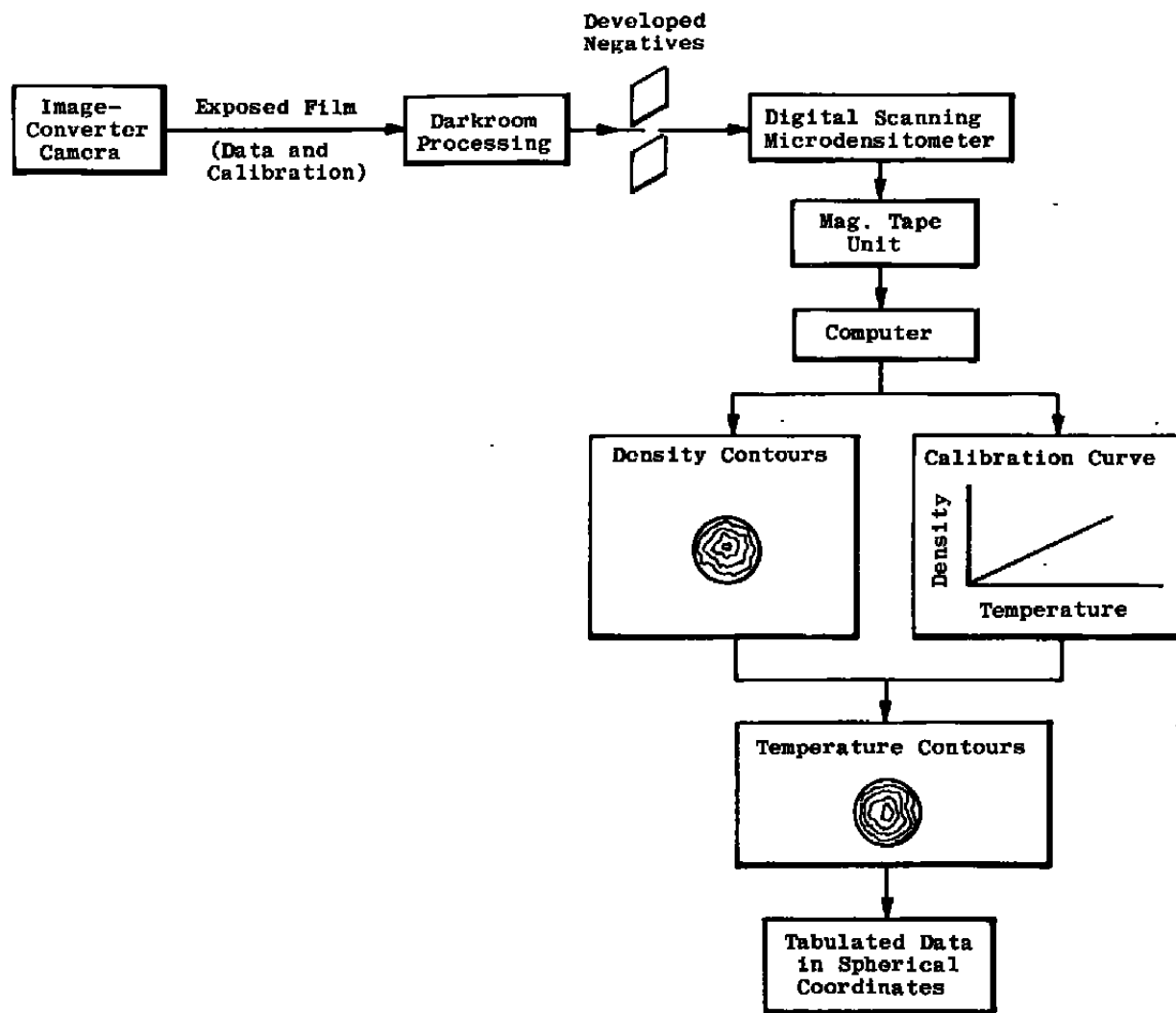
Figure 5.   Surface temperature data reduction flow chart.
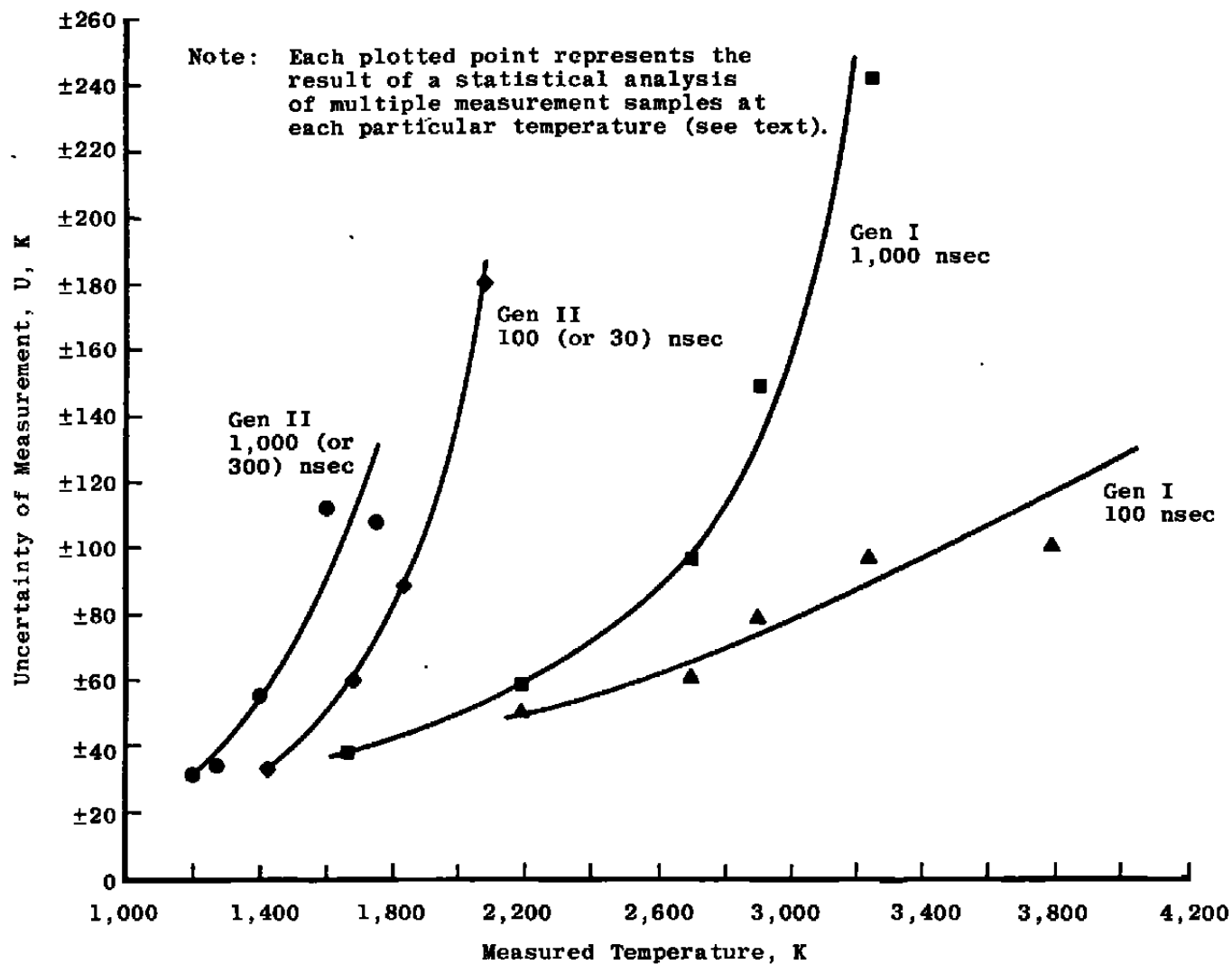
Figure 6.   Photopyrometer temperature measurement uncertainty.
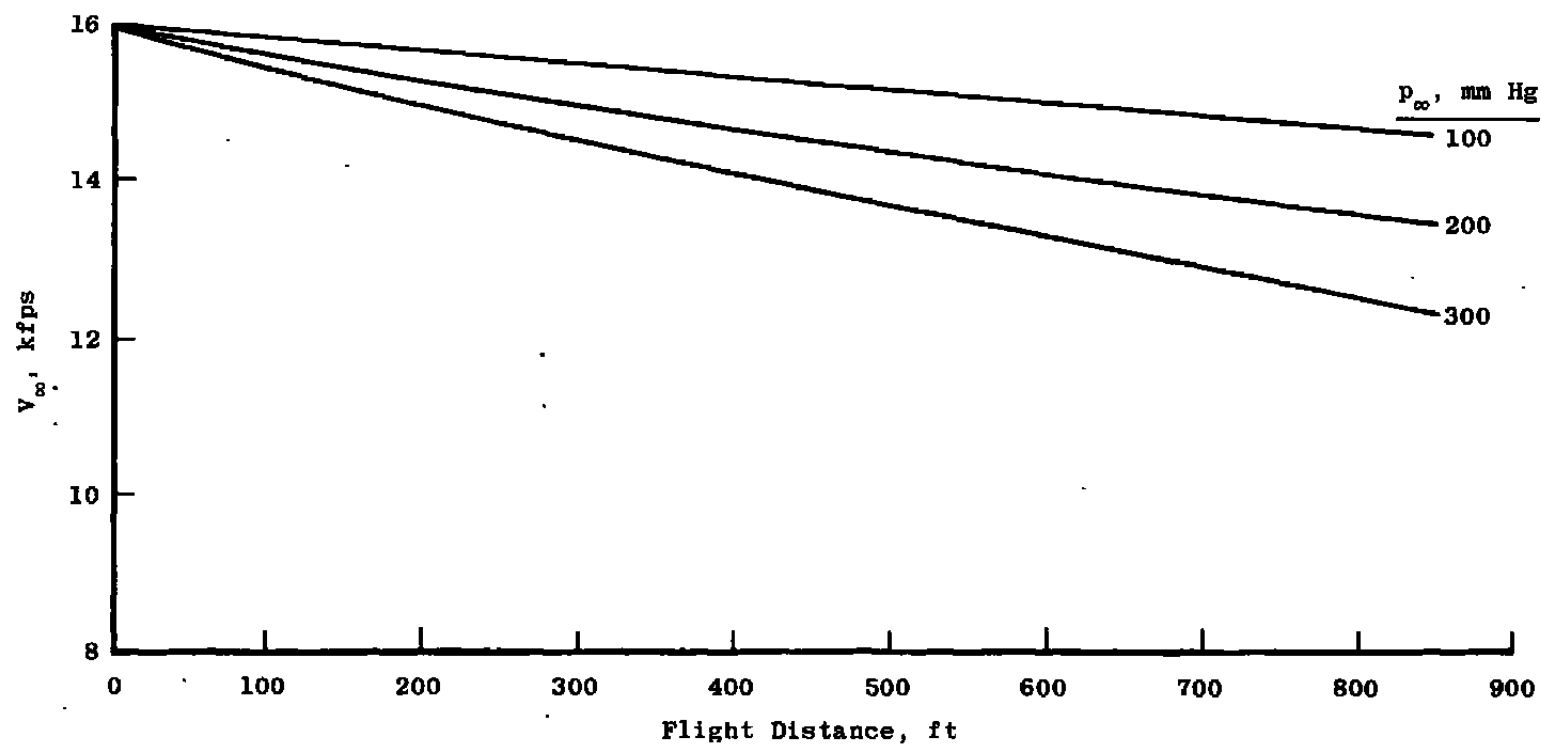
Figure 7.   Velocity decay for large nosetip model.
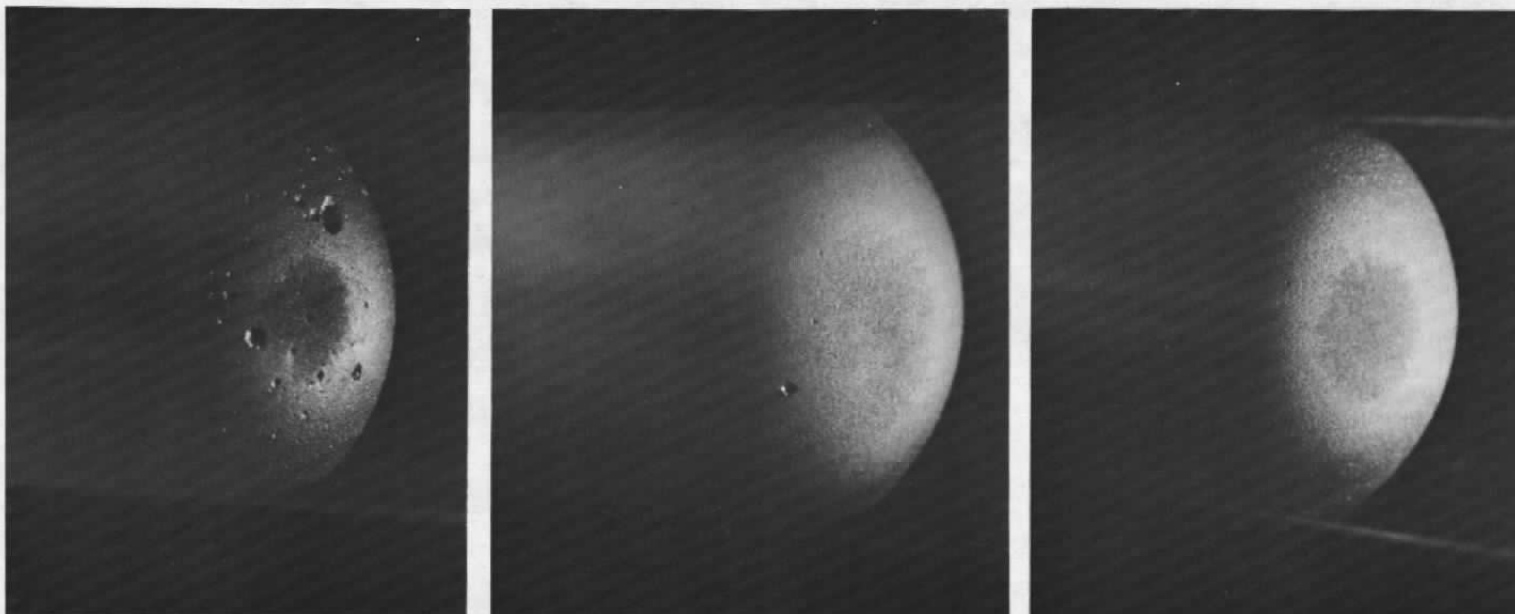
a. Heavily damaged,
   Shot No. 5,015

b. Slightly damaged,
   Shot No. 5,038

c. Undamaged, Shot No. 5,045

Figure 8.   In-flight photographs of nosetips.
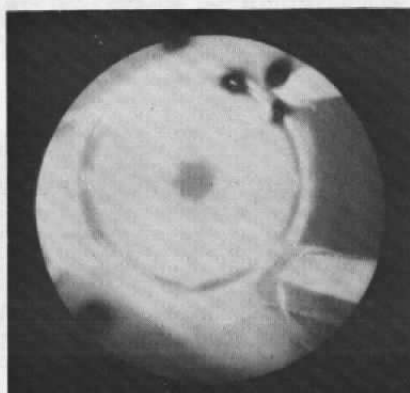
STA 11, 238 ft   STA 20, 398 ft   STA 29, 596 ft   STA 41, 836 ft
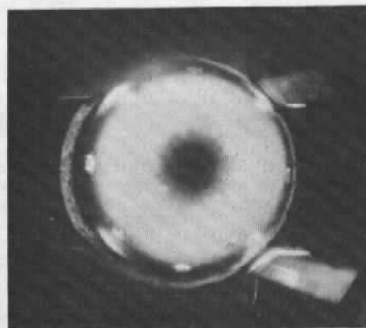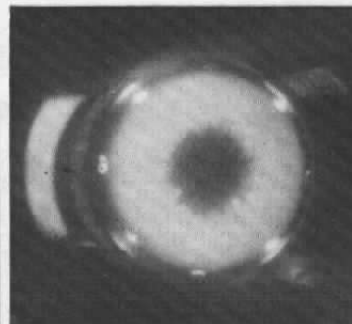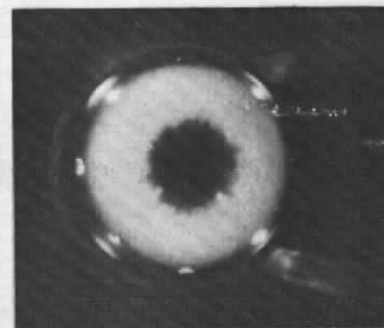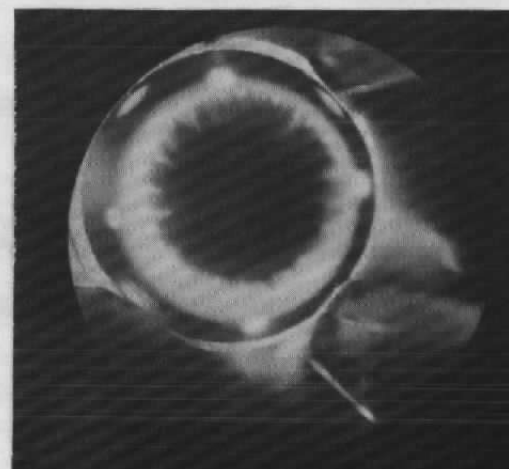
Note: STA = Range Station

a. Shot 5,014
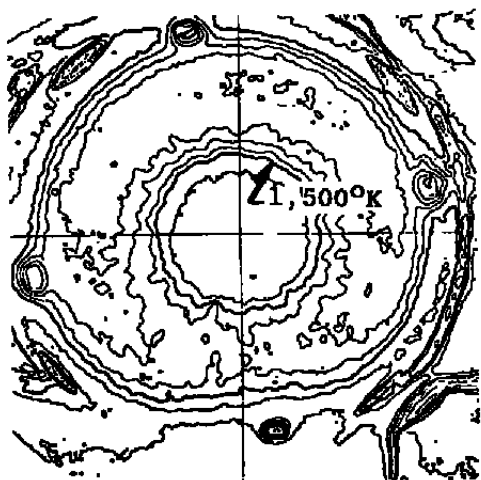Figure 9. Typical image-converter camera photographs.
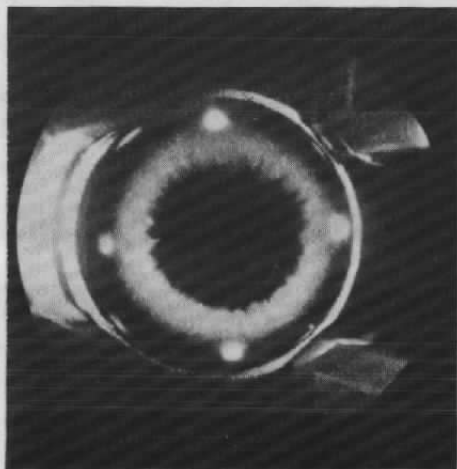
STA 20, 398 ft   STA 29, 596 ft   STA 41, 836 ft
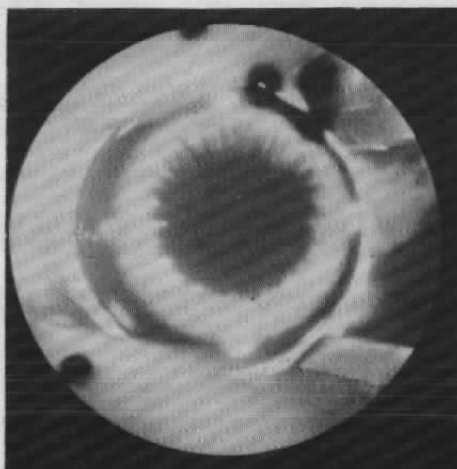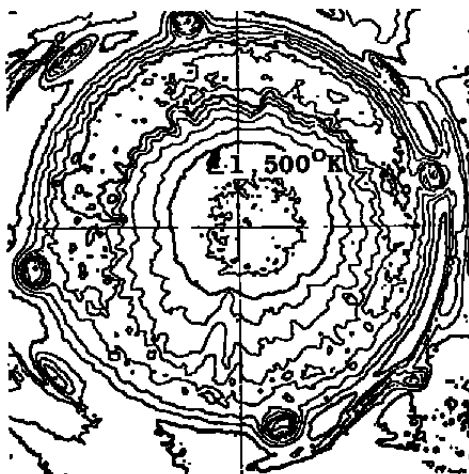
Note: STA = Range Station

b.   Shot 5,027
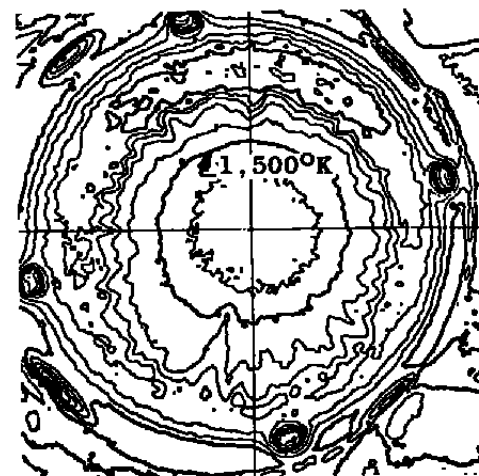Figure 9.   Concluded.

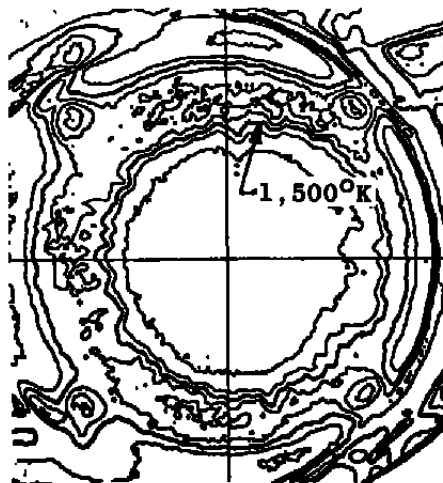STA 20, 398 ft   STA 29, 596 ft   STA 41, 836 ft
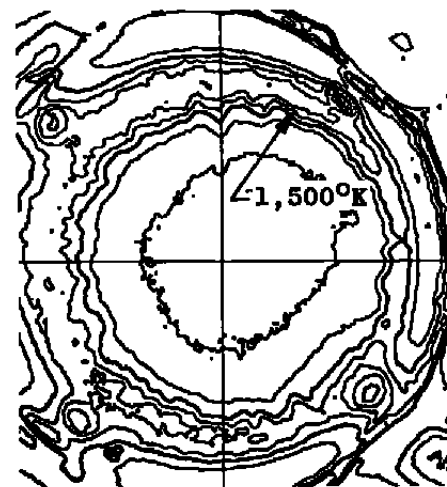
a.   Shot No. 5,024, contour interval 100°K
Figure 10.   Example of temperature data in spherical coordinates.

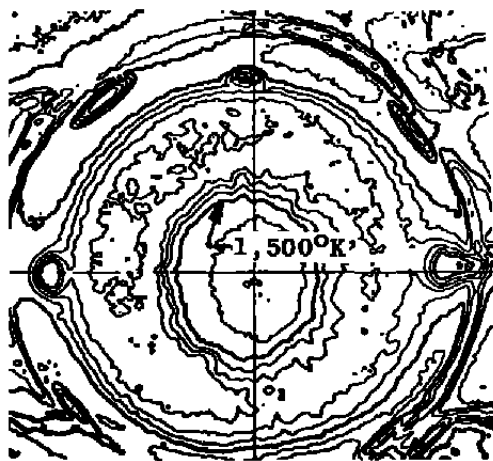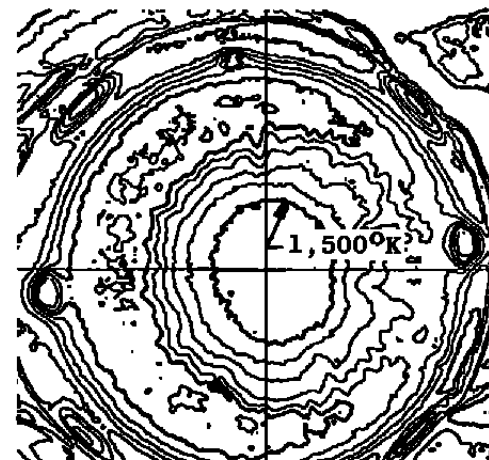STA 20, 398 ft   STA 29, 596 ft   STA 41, 836 ft

b. Shot No. 5,037, contour interval 100°K
Figure 10.   Continued.

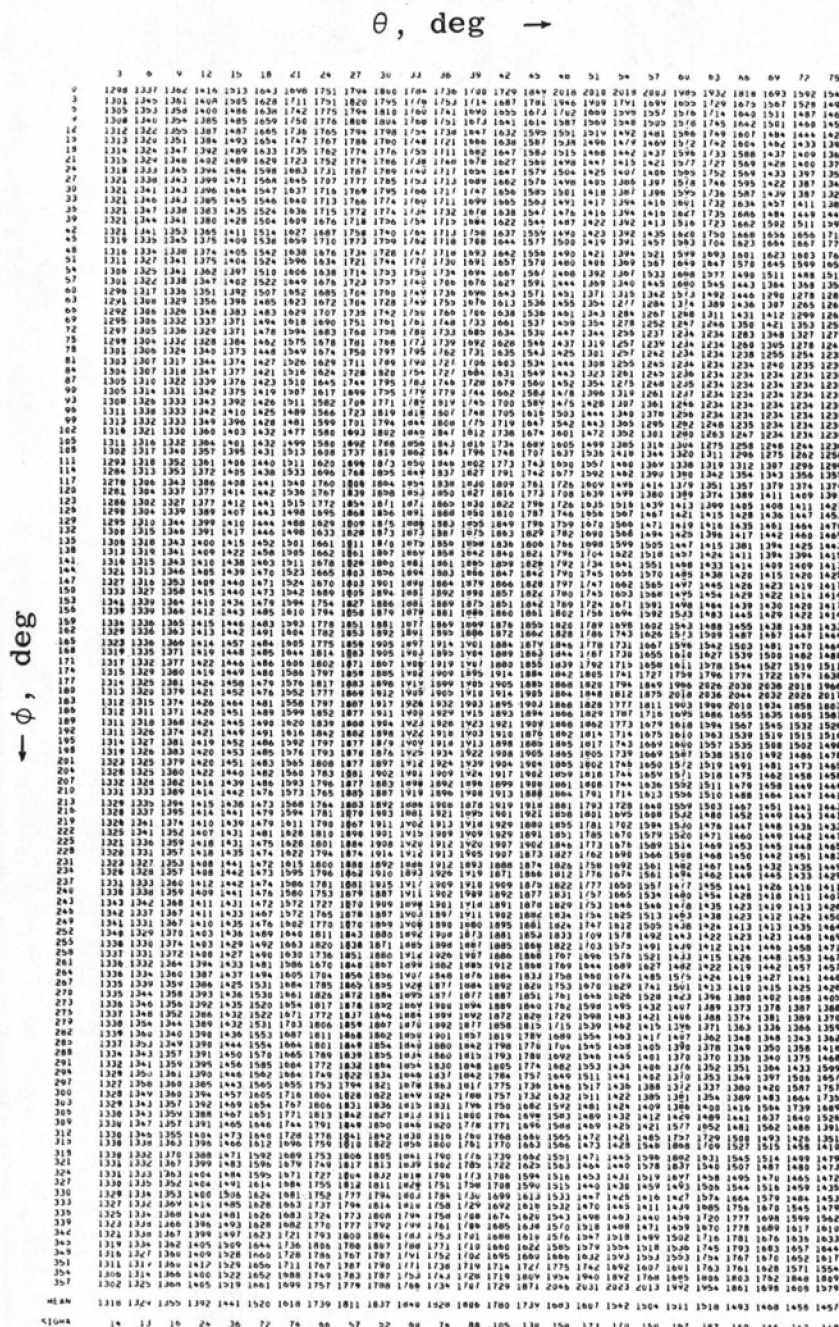STA 20, 398 ft   STA 29, 596 ft   STA 41, 836 ft

c. Shot No. 5,045, contour interval 100° K
Figure 10.   Concluded.

θ, deg →

Shot No. 5,045, STA 20

Figure 11. Tabulated temperature data in spherical coordinates.

34

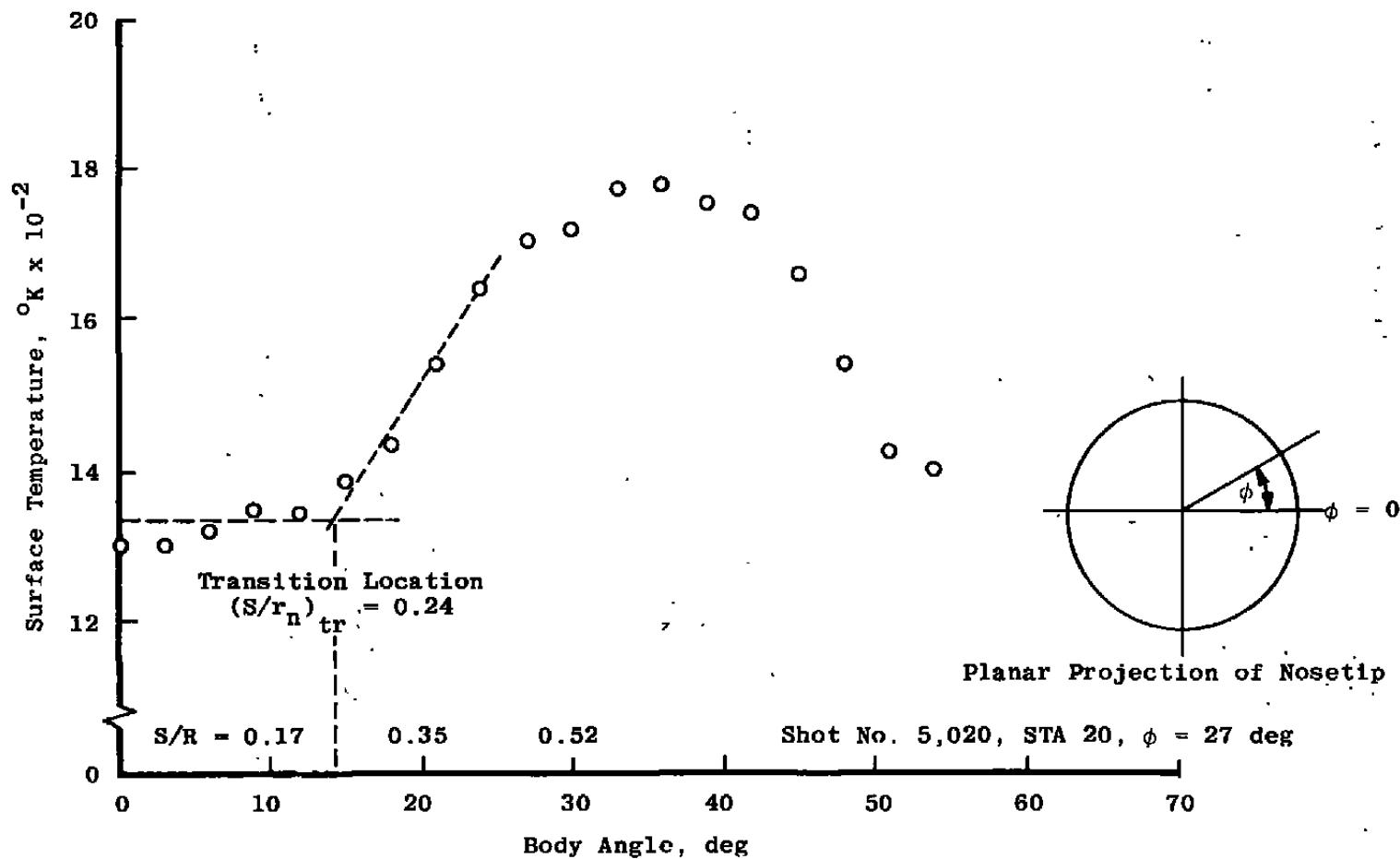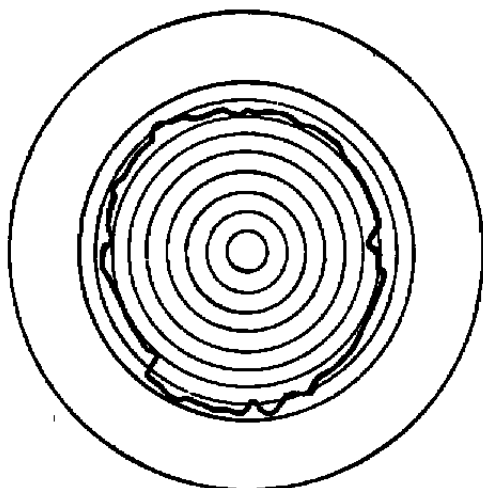Figure 12. Example of temperature distribution and
definition of transition location.

Circles Every 5 deg to 45,
Plus 90-deg Circle

a. Shot No. 5,021, STA 29
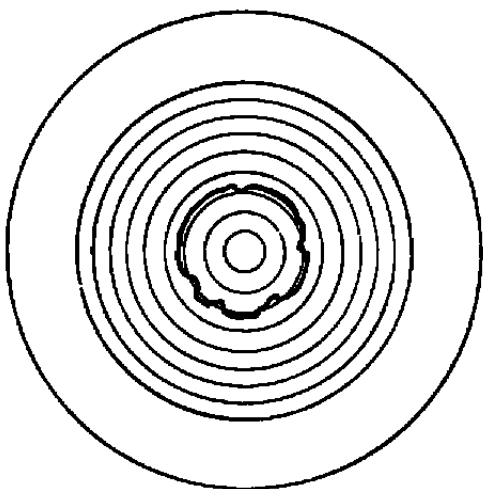
b. Shot No. 5,024, STA 20
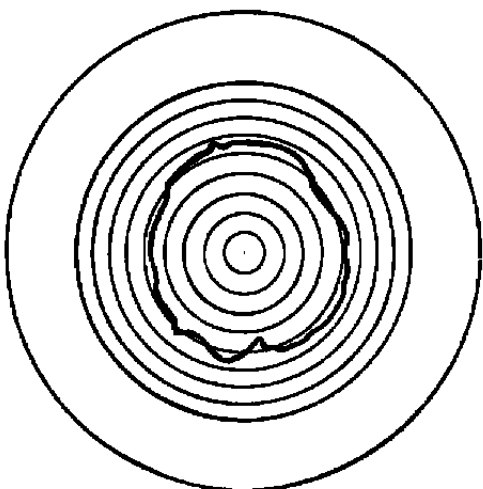
c. Shot No. 5,037, STA 29

Figure 13. Planar projection of transition front location.
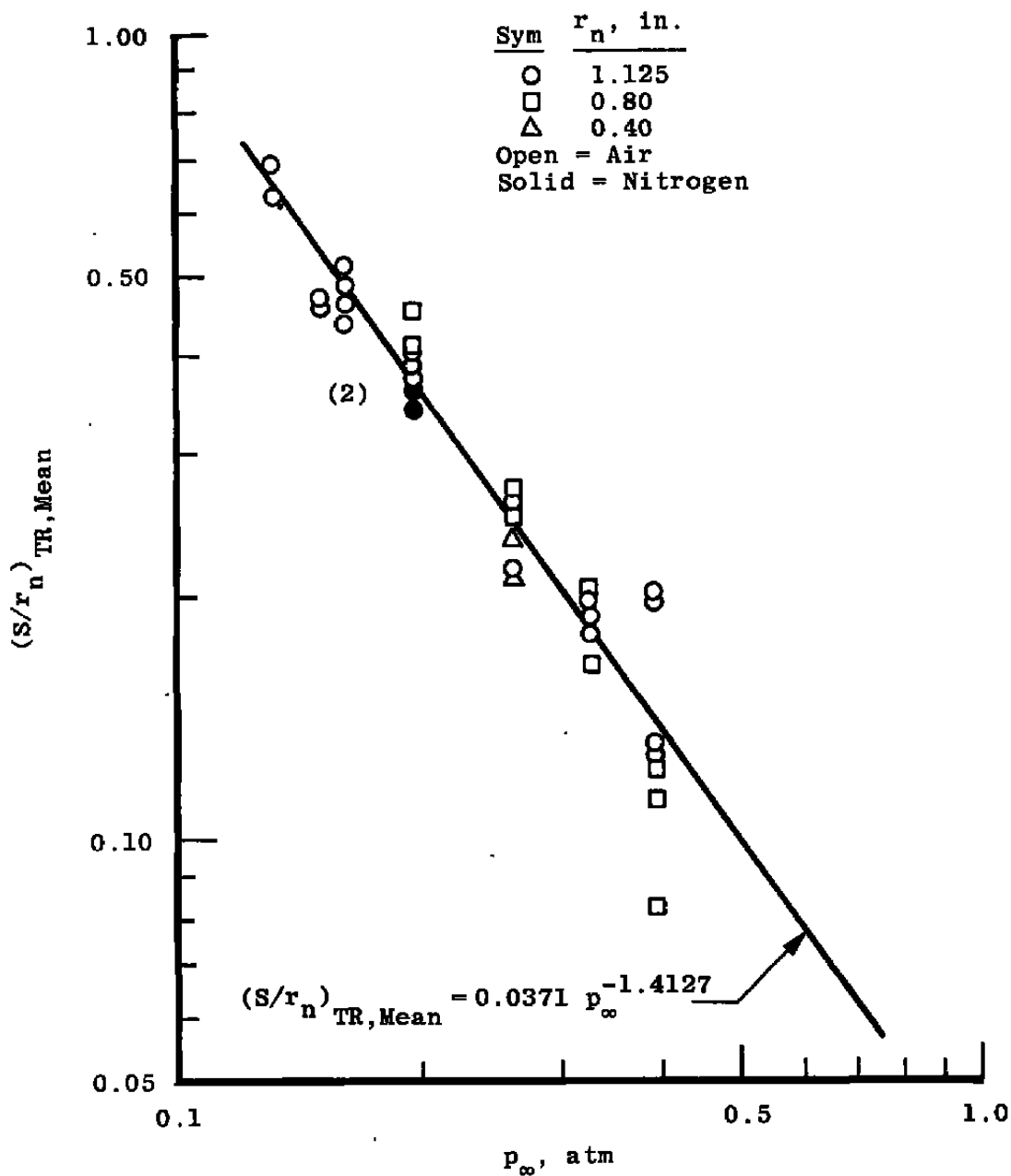
Figure 14. Variation of mean transition location with range pressure.

Figure 15.   Measurements of transition zone asymmetry.

Table 1. Nominal Measurement Ranges for Photopyrometers

System Designation	Number in Use	Exposure Duration, msec	Dynamic Range, °K
Gen-I	3	1,000	1,600 – 3,300
		100	1,950 – 4,000
Gen-II	2	1,000	1,250 – 1,900
		100	1,500 – 2,400
Gen-II	1	300	1,250 – 1,900
		30	1,500 – 2,400

Table 2. Test Summary

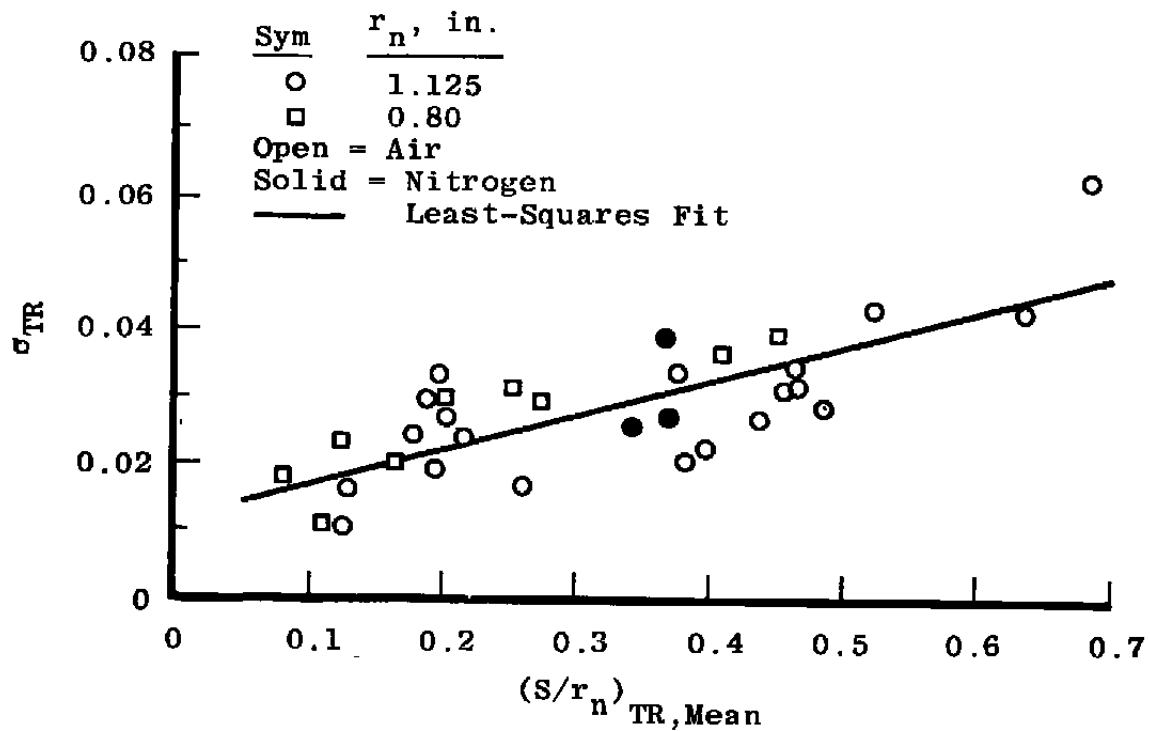| Shot No.	r_n, in.	p_∞, torr	Nosetip Recovery	Comments
4,975	1.125	200	No	Model development — no data reported.
4,985	1.125	200	Yes	Model development — no data reported.
4,995	0.80	200	No	Model development — no data reported.
5,000	0.43	200	Yes	
5,001	1.125	300	----	No data — nosetip failed during launch.
5,002	1.125	300	----	No data — nosetip failed during launch.
5,014	1.125	300	No	Low launch velocity (14,780 fps).
5,015	1.125	200	No	No data — nosetip damaged at range entrance.
5,016	1.125	150	No	Low launch velocity (14,460 fps).
5,017	1.125	200	----	No data — nosetip disintegrated in flight.
5,019	1.125	150	No	
5,021	1.125	100	No	
5,024	1.125	200	Yes	
5,027	1.125	125	No	
5,028	0.80	200	Yes	
5,031	0.80	150	Yes	
5,032	0.80	250	No	
5,033	0.80	300	No	
5,037	1.125	125	Yes	
5,038	1.125	125	Yes	
5,043	1.125	150	No	No data — nosetip damaged at range entrance.
5,044	1.125	150	No	
5,045	1.125	200	No	
5,054	1.125	150	Yes	N_2 test gas.
5,055	1.125	250	Yes	
5,056	1.125	115	" No	No data — low launch velocity, temperatures below system thresholds.
5,063	1.125	115	Yes	

Table 3. Model Angle Data

Shot No.	Pitch Plane Angle, deg							Yaw Plane Angle, deg		
	Distance Downrange, ft ➔									
	76	156	226	383	478	583	703	59	318	823
5,000	0.0	−0.4	−0.1	−1.6	−0.5	−1.0	−1.5	0.0	----	−0.3
5,014	−0.2	−0.5	−0.6	−0.6	−0.5	0.0	0.0	0.5	2.0	−1.1
5,016	0.5	−0.5	0.6	−0.6	----	0.5	0.0	1.0	1.6	−1.6
5,019	0.4	−0.8	1.4	−1.0	−0.4	0.9	0.9	0.8	1.5	−1.0
5,021	0.0	−1.4	0.3	−0.9	−0.3	−0.4	0.1	−0.5	0.9	−1.0
5,024	0.4	−1.0	−1.2	−3.3	−0.2	−0.2	0.3	−0.5	0.5	−0.3
5,027	0.0	−0.4	−0.5	−1.6	−0.7	−0.5	0.7	−0.5	1.3	0.9
5,028	----	−0.7	−0.6	0.2	−0.3	0.5	1.3	−0.6	1.5	0.3
5,031	0.5	----	−0.9	0.0	0.3	0.9	0.5	----	1.3	0.8
5,032	0.6	−0.9	−1.1	−0.1	1.1	1.9	−0.2	−0.4	1.1	1.3
5,033	0.2	−0.4	−0.3	0.5	0.0	0.9	1.0	0.9	1.8	−0.3
5,037	−0.2	−0.9	1.0	0.8	1.7	1.4	1.8	−0.5	1.8	−0.2
5,038	0.0	−0.3	0.7	−1.8	−0.4	2.5	−1.2	−0.3	2.5	0.7
5,044	−0.8	−1.3	−0.5	−2.4	−2.0	−1.6	0.1	0.0	0.6	−0.3
5,045	−1.0	1.0	1.2	−2.9	−0.7	1.2	1.7	1.0	1.3	−1.3
5,054	−0.5	−0.5	−1.6	−2.4	−0.5	−0.7	1.5	0.6	1.4	2.8
5,055	−1.1	−0.2	1.0	−2.3	−0.5	−0.7	1.0	1.0	1.1	1.1
5,063	0.1	−0.8	0.9	−1.1	2.0	2.1	−1.0	−0.3	1.6	0.5
Mean	|0.4|	|0.7	|0.8|	1.3	0.7	|1.0|	|0.8|	|0.5|	|1.4|	|0.9|

NOMENCLATURE

A   Model base area, ft^2

C_D Drag coefficient

p_∞ Free-stream pressure, torr

r_n Nose radius, in.

S   Surface distance, in.

T   Temperature, °K

V   Velocity, fps

w   Model weight, lb

x   Distance down range, ft

β Ballistic coefficient, $w_{C_{DA}}lb/ft^2$

θ Angular location on surface in flow direction, deg

σ_{tr} Standard deviation of $(S/r_n)_{tr}$ measurements (at 3-deg intervals around the nose)

ϕ Angular location in circumferential direction around nosetip, deg

SUBSCRIPTS

i   Initial

tr   Transition location

∞ Free stream